doi:10.1093/brain/awx249 BRAIN 2017: 140; 2838–2850 | 2838

BRAIN
A JOURNAL OF NEUROLOGY

Choline transporter mutations in severe congenital myasthenic syndrome disrupt transporter localization

Haicui Wang,[1,2,*] Claire G. Salter,[3,4,*] Osama Refai,[5,*] Holly Hardy,[3] Katy E. S. Barwick,[3] Ugur Akpulat,[1,2,6] Malin Kvarnung,[7,8] Barry A. Chioza,[3] Gaurav Harlalka,[3] Fulya Taylan,[7,9] Thomas Sejersen,[9,10] Jane Wright,[11] Holly H. Zimmerman,[12] Mert Karakaya,[2] Burkhardt Stüve,[13] Joachim Weis,[14] Ulrike Schara,[15] Mark A. Russell,[3] Omar A. Abdul-Rahman,[16] John Chilton,[3] Randy D. Blakely,[5] Emma L. Baple,[3] Sebahattin Cirak[1,2,#] and Andrew H. Crosby[3,#]

[*,#]These authors contributed equally to this work.

The presynaptic, high-affinity choline transporter is a critical determinant of signalling by the neurotransmitter acetylcholine at both central and peripheral cholinergic synapses, including the neuromuscular junction. Here we describe an autosomal recessive presynaptic congenital myasthenic syndrome presenting with a broad clinical phenotype due to homozygous choline transporter missense mutations. The clinical phenotype ranges from the classical presentation of a congenital myasthenic syndrome in one patient (p.Pro210Leu), to severe neurodevelopmental delay with brain atrophy (p.Ser94Arg) and extend the clinical outcomes to a more severe spectrum with infantile lethality (p.Val112Glu). Cells transfected with mutant transporter construct revealed a virtually complete loss of transport activity that was paralleled by a reduction in transporter cell surface expression. Consistent with these findings, studies to determine the impact of gene mutations on the trafficking of the *Caenorhabditis elegans* choline transporter orthologue revealed deficits in transporter export to axons and nerve terminals. These findings contrast with our previous findings in autosomal dominant distal hereditary motor neuropathy of a dominant-negative frameshift mutation at the C-terminus of choline transporter that was associated with significantly reduced, but not completely abrogated choline transporter function. Together our findings define divergent neuropathological outcomes arising from different classes of choline transporter mutation with distinct disease processes and modes of inheritance. These findings underscore the essential role played by the choline transporter in sustaining acetylcholine neurotransmission at both central and neuromuscular synapses, with important implications for treatment and drug selection.

1 University Hospital Cologne, Department of Pediatrics, Kerpener Str. 62, 50937 Cologne, Germany
2 Center for Molecular Medicine Cologne (CMMC), University of Cologne, Robert-Koch-Str. 21, 50931 Cologne, Germany
3 RILD Wellcome Wolfson Centre, Royal Devon and Exeter NHS Foundation Trust, Barrack Road, Exeter, EX2 5DW, UK
4 Human Genetics and Genomic Medicine, Faculty of Medicine, University of Southampton, Southampton, SO16 6YD, UK
5 Department of Biomedical Science, Charles E. Schmidt College of Medicine and Brain Institute, Florida Atlantic University, Jupiter, FL, USA
6 Kastamonu University, 37150 Kastamonu, Turkey
7 Department of Molecular Medicine and Surgery, Center for Molecular Medicine, Karolinska Institutet, 17176 Stockholm, Sweden
8 Department of Clinical Genetics, Karolinska University Hospital, 17176 Stockholm, Sweden
9 Science for Life Laboratory, Karolinska Institutet Science Park, 17121 Stockholm, Sweden

Received April 21, 2017. Revised August 3, 2017. Accepted August 5, 2017

10 Department of Women's and Children's Health, Division of Pediatric Neurology, Karolinska Institutet, 17176 Stockholm, Sweden
11 Department of Pharmacology, Vanderbilt University, Nashville, TN, USA
12 Division of Medical Genetics, University of Mississippi Medical Center, Jackson, Mississippi 39216, USA
13 Children's Hospital Social Pediatric Center, 50735 Cologne, Germany
14 Institute of Neuropathology and Jülich Aachen Research Alliance (JARA) Brain Translational Medicine, RWTH Aachen University, 52074 Aachen, Germany
15 University Children's Hospital Essen, Essen, Germany
16 Department of Pediatrics, University of Mississippi Medical Center, Jackson, Mississippi 39216, USA

Correspondence to: Prof Andrew Crosby
RILD Wellcome Wolfson Centre
Royal Devon and Exeter NHS Foundation Trust
Barrack Road, Exeter, EX2 5DW, UK
E-mail: A.H.Crosby@Exeter.ac.uk

Correspondence may also be addressed to: Dr Sebahattin Cirak
University Hospital Cologne, Department of Pediatrics
Center for Molecular Medicine Cologne
University of Cologne, 50937, Cologne, Germany
E-mail: sebahattin.cirak@uk-koeln.de

Keywords: *SLC5A7*; CHT; congenital myasthenic syndrome; choline uptake; CHT trafficking

Abbreviations: CHT = choline transporter; CMS = congenital myasthenic syndrome; dHMN = distal hereditary motor neuropathy; NMJ = neuromuscular junction

Introduction

Synaptic signalling by the neurotransmitter acetylcholine at the neuromuscular junction (NMJ) and central synapses are essential for movement and for multiple aspects of cognitive function (Sarter *et al.*, 2005) and reward (McKay *et al.*, 2007). An expanding number of inherited diseases affecting cholinergic synapses have been characterized over recent years (Engel *et al.*, 2015), mostly affecting the neuromuscular endplate, which are associated with variable fatigability of skeletal muscle and weakness. They are classified under the term 'congenital myasthenic syndromes' (CMS). A precise molecular diagnosis of CMS is essential to aid successful and safe treatment, related to the specific functional consequence arising from gene mutation. Most forms of CMS are caused by gene mutations that result in postsynaptic defects, which are commonly associated clinically with ptosis, ophthalmoplegia and fatigability. Conversely, presynaptic defects may exhibit remarkably different phenotypes due to dysfunction of CNS cholinergic synapses, including apnoeic attacks associated with choline acetyltransferase (*CHAT*) mutations (Arredondo *et al.*, 2015), and motor neuropathy associated with synaptotagmin 2 (*SYT2*) mutations (Herrmann *et al.*, 2014). The importance of cholinergic synapses for central neurotransmission is further reflected by the complex phenotype of myasthenia, epilepsy, ataxia and intellectual disability associated with mutations in the synaptosomal-associated protein of 25 kDa (*SNAP25*) (Shen *et al.*, 2014). These heterogeneous yet overlapping clinical manifestations highlight the importance of deciphering the specific underlying genetic and molecular defects responsible for cholinergic synapse malfunction. In turn, this will provide an improved understanding of the biological role of the presynaptic machinery and aid the development of more effective treatments for cholinergic synapse disorders.

Major sites of peripheral cholinergic signalling include the pre- and postganglionic synapses of the parasympathetic nervous system, the preganglionic synapses of the sympathetic nervous system, and the NMJ (Engel *et al.*, 2015). The NMJ is a complex cellular structure formed through the interaction of three main structural components including the motor nerve terminal, the postsynaptic muscle membrane, and the synapse-associated terminal Schwann cells (Feng and Ko, 2008). Transmission of an electrical impulse across the NMJ is achieved through the release of acetylcholine neurotransmitter contained within presynaptic vesicles, which are stored at the presynaptic nerve terminal until cell membrane depolarization stimulates acetylcholine release into the synaptic cleft. Acetylcholine is cleaved back into its two component molecules, acetate and choline, by the action of acetylcholinesterase (AChE, encoded by *ACHE*). Choline is efficiently recovered through uptake by the presynaptic, hemicholinium-3 (HC-3) sensitive, choline transporter (CHT, *SLC5A7*), through which it may re-enter the acetylcholine biosynthetic pathway. CHT forms a dimer (Okuda *et al.*, 2012) and is predominantly located in intracellular endosome and synaptic vesicles in the cell body and also neurites, as demonstrated in cultured neuronal cells *in vitro* (Ribeiro *et al.*, 2003, 2005, 2007) and in cholinergic synapses in brain (Ferguson *et al.*, 2004; Nakata *et al.*, 2004).

About 10% of total CHT in cells forms a rapid recycling pool as a physiological reserve, and Ca^{2+} dependent K^+ depolarization may promote the rate of recycling of CHT to the plasma membrane to enable rapid choline uptake (Ferguson *et al.*, 2003; Ribeiro *et al.*, 2007).

Previously we investigated the genetic and molecular basis of a form of autosomal dominant distal hereditary motor neuropathy associated with vocal cord paralysis (dHMN-VII) present in multiple individuals in a large UK family. These studies determined that a dominantly-acting, frameshift *SLC5A7* mutation disrupted the C-terminus of CHT and led to significantly impaired, but not completely abrogated, transporter activity. Here we identified patients with a different class of *SLC5A7* mutation, associated with an autosomal recessive mode of inheritance and disease mechanism, which is associated with the more severe clinical outcome of CMS. These findings were defined independently and in parallel with those of a recent study identifying autosomal recessive CHT mutation in CMS (Bauché *et al.*, 2016). Our study supports and extends these findings clinically and functionally, and determines that dominantly- and recessively-acting CHT mutations may lead to variably impaired CHT functionality through a combined effect on both CHT specific activity, as well as alterations of protein transport to the NMJ, leading to distinct clinical outcomes.

Materials and methods

Genetic studies

Genomic DNA samples were extracted from peripheral blood following standard protocols. Whole exome sequencing was performed following exome enrichment using an Illumina HiSeq 2000 (Yis *et al.*, 2016; Ahmed *et al.*, 2017). Reads were analysed for exome coverage, SNP/InDel variant calling and quality assessment, resulting in >95% of targeted sequences covered for variant calling at >10× coverage in each case. Filtering involved common variants [>1% in 1000 Genomes http://browser.1000genomes.org, NHLBI Exome Variant Server http://evs.gs.washington.edu/EVS, Exome Aggregation Consortium http://exac.broadinstitute.org, and the Greater Middle Eastern (GME) Variome Database http://igm.ucsd.edu/gme/index.php] and homozygous recessive inheritance. Oligonucleotide primers for dideoxy sequence validation (using Applied Biosystems 3130 DNA Sequencer, Life Technologies) were designed using Primer3 online tool (http://bioinfo.ut.ee/primer3-0.4.0/) with oligonucleotide primer sequence specificity verified by using the UCSC In-Silico PCR tool, and sequences screened to exclude common single nucleotide polymorphisms.

Expression vectors

The *SLC5A7* cDNA (NM_020815) was purchased from Origene in pCMV6-Entry vector with a myc/DDK tag in the C-terminus. N-terminal haemagglutinin (HA)-tagged construct was the same as that used in our previous study (Barwick *et al.*, 2012). Missense mutations within the *SLC5A7* cDNA sequence were introduced via Q5® Site-Directed Mutagenesis Kit (NEB), and confirmed by dideoxy sequencing (GATC). All plasmid DNAs were isolated using Qiagen Maxi Kit.

Cell culture and transfection

HEK 293T cells were cultured in Dulbecco's modified Eagle medium (DMEM) (Thermo Fisher Scientific), 10% foetal bovine serum (Biochrom), and penicillin-streptomycin (Thermo Fisher Scientific). For transfections, 60–80% confluent cells were transfected by PEI (polyethylenimine, Sigma) for surface protein ELISA assay or Lipofectamine™ 3000 (Thermo Fisher Scientific) for surface protein isolation assay and immunostainings. PC12 cells were cultured in DMEM plus GlutaMAX™-I, (ThermoFisher Scientific), 10% horse serum and 5% foetal bovine serum (Biochrom), and penicillin-streptomycin. For transfections of PC12 cells, 60–70% confluent cells were transfected with Lipofectamine™ 3000.

Surface protein isolation

Surface CHT protein isolation was performed using the Surface Protein Isolation Kit (Pierce) following manufacturer's instructions. Briefly, equal numbers of HEK 293T cells were seeded in 10 cm diameter dishes 24 h before transfection, with duplicates for each construct. Then 60–80% confluent cells were transfected by Lipofectamine™ 3000 (Thermo Fisher Scientific) with equal amounts of DNA construct expressing C-terminal myc-tagged wild-type or mutant CHT. Cells were biotinylated 24 h later by biotinylation reagent (Sulfo-NHS-SS-Biotin) on ice for 30 min prior to quenching and cell scraping pelleting and lysis. Equal amounts of total cell lysates were applied to equal amounts of NeutrAvidin™ resin to isolate the biotinylated surface proteins.

Equal amounts of SDS-PAGE sample buffer (62.5 mM Tris-HCl pH6.8, 1% SDS, 10% glycerol, 50 mM DTT) were used to elute each sample from the resins at 4°C overnight. Meanwhile total cell lysate diluted in SDS-PAGE sample buffer was incubated at 4°C overnight as described previously (Holmstrand *et al.*, 2014). Protein samples were boiled at 50°C for 15 min then subjected to 4–12% Bis-Tris gel electrophoresis (Thermo Fisher Scientific) following transfer to nitrocellulose membrane. Western blotting was performed with myc-HRP antibody (1:2000, Miltenyi Biotec) to detect CHT-myc and GAPDH as input control of total lysate (mouse anti-GAPDH, 1:200 Santa-Cruz).

Surface protein ELISA

The expression level of total or surface wild-type or mutant CHT was evaluated by ELISA as described in Bogatcheva *et al.* (2007). Briefly, equal numbers of HEK 293T cells were plated 24 h before transfection in 24-well plates coated with poly-L-lysine (0.1 mg/ml). Then cells (60–70% confluent) were transfected by PEI with DNA constructs (500 ng per well) expressing N-terminal HA-tagged wild-type or mutant CHT. For analysis, cells were washed with phosphate-buffered saline (PBS) and fixed with 3.7% formaldehyde after 24 h transfection, following permeabilization with 0.25% Triton™ X-100 to detect total HA-CHT or without permeabilization to detect surface HA-CHT. After blocking with 1% bovine serum

albumin (BSA) in PBS, cells were then incubated with anti-HA-HRP antibody (Miltenyi Biotec, 1:2000) for 1 h at room temperature. Cells were washed three times with PBS, and then colorimetric HRP substrate TMB (3,3',5,5'-tetramethylbenzidine, Sigma) was added. The reaction was stopped by placing cells on ice immediately once adequate colour was achieved. The supernatants were read at 655 nm in a 96-well plate with a microplate reader (Tecan). The values resulting from cells transfected with wild-type or mutant CHT were subtracted by the baseline value of non-transfected cells.

Evaluation and quantification of mutant CHT expression in HEK 293T cells

HEK 293T cells were seeded on 12-well plates coated with poly-L-lysine (0.1 mg/ml) 24 h before transfection. At 60–70% confluency, cells in each well were transfected with 1 µg DNA construct expressing C-terminal myc-tagged wild-type or mutant CHT (for quantification), or together with 1 µg vector expressing GFP-Lamp1 (gift from Natalia Kononenko Lab, CECAD cologne). Twenty-four hours later cells were fixed for staining. For Lamp1 co-localization, images were taken by FV-1000 confocal microscope, with imaging for quantification in wide field (Olympus IX 81).

CHT intracellular vesicle analysis in PC12 cells

PC12 cells were seeded on 12-well plates with coverslips coated with collagen G (30 µg/ml; Merck Millipore). At 60–70% confluency, cells were transfected with 1.6 µg DNA construct per well expressing C-terminal myc-tagged wild-type or mutant CHT by Lipofectamine™ 3000 (Thermo Fischer Scientific). For co-transfection with construct expressing GFP-Lamp1 or GFP-Rab7, 800 µg of CHT-myc construct and 800 µg GFP-Lamp1 or GFP-Rab7 constructs were used. Forty-eight hours after transfection, cells were fixed for immunostaining.

Immunostaining

Both HEK 293T cells and PC12 cells were fixed in 3.7% formaldehyde in PBS for 15 min at room temperature and rinsed in PBS. Cells were permeabilized in PBS containing 0.25% Triton™ X-100 for 10 min at room temperature and rinsed in PBS again prior to incubation with blocking buffer (1% BSA in PBS + Tween 0.1% as PBST) for 30 mins to block non-specific binding of antibodies. Primary antibodies were added at the appropriate dilution in blocking buffer to cells for 1 h incubation at room temperature. After washing in PBS, cells were incubated with secondary antibodies together with DAPI for 1 h at room temperature in the dark. After the washing in PBS, coverslips were mounted in mounting medium (Polysciences) and fluorescent images were captured on an Olympus Fluoview FV 1000 (for fine cellular structure visualization) and Olympus IX 81 (for quantification). Analysis of fluorescence intensities was performed with ImageJ software.

Antibodies used for immunostaining: mouse anti-c-myc (1:200, Santa Cruz), rabbit anti-c-myc (1:200, Cell Signaling), mouse anti-Synapsin 1a/b (1:200, Santa Cruz), rabbit anti-Protein Disulfide Isomerase (anti-PDI) (1:100, sigma), rabbit anti-Golga2 (1:200, Sigma), Alexa Fluor® 448 or 594 goat anti-mouse IgG (H + L) and Alexa Fluor® 448 or 594 goat anti-rabbit IgG (H + L) (1:200, ThermoFischer Scientific), Alexa Fluor® 488 goat anti-mouse IgG/IgM (H + L) (1:200, ThermoFischer Scientific).

Caenorhabditis elegans transgenics and transport assays

Somatic export of the CHT orthologue CHO-1 to cholinergic synapses *in vivo* was performed using $P_{cho\text{-}1}$::CHO-1::GFP as previously described (Matthies *et al.*, 2006) using an expression construct that consists of the *cho-1* native promoter (7.6 Kb upstream of ATG start site), the genomic sequence of *cho-1* gene, and a C-terminal GFP tag. Point mutants p.Ser94Arg and p.Ile112Glu were introduced into *cho-1* by mutagenesis (New England Biolabs Q5® Site-Directed Mutagenesis Kit). Transporter expression was examined after injecting wild-type or mutant constructs, independently, into wild-type worms (N2) at 20 ng/µl, followed by crossing these lines into *cho-1*(*tm373*) animals that possess a loss of function allele (confirmed by PCR genotyping). Synaptic localization of CHO-1 in cholinergic neurons was evaluated by mCherry::RAB-3 expression driven by the *acr-2* promoter that is specific to cholinergic neurons, using plasmid pPRB47 ($P_{acr\text{-}2}$::mCherry::RAB-3) (a gift from Michael M. Francis, University of Massachusetts). Imaging was undertaken in young adult hermaphrodite worms using a Nikon A1R confocal laser microscope at the FAU Nikon Center of Excellence.

CHT transporter activity assays

We investigated the outcome of the missense sequence variants on CHT transporter activity using ^{3}H-choline transport assays as described previously, using HEK 293T cells transiently transfected by N-terminal haemagluttinin (HA)-tagged transporters for cell-surface biotinylation experiments (Barwick *et al.*, 2012).

Results

Clinical findings

We investigated four individuals from three nuclear families (Fig. 1 and Table 1) presenting in the newborn period with a common clinical phenotype of generalized hypotonia, respiratory insufficiency and apnoea's, bulbar and extra-ocular muscle involvement, generalized muscle weakness, fatigability and a decrement of the electrical muscle response on nerve stimulation, all consistent with a presynaptic CMS-like disorder. All affected individuals displayed severe-profound global developmental delay. The most severe clinical outcome observed was early infantile lethality in both affected children in Family 2 (Patients V:1 and V:3). Patient IV:1 of Family 1 had not achieved any developmental milestones within the speech, cognitive or motor domains by the age of 2.5 years, there were minimal

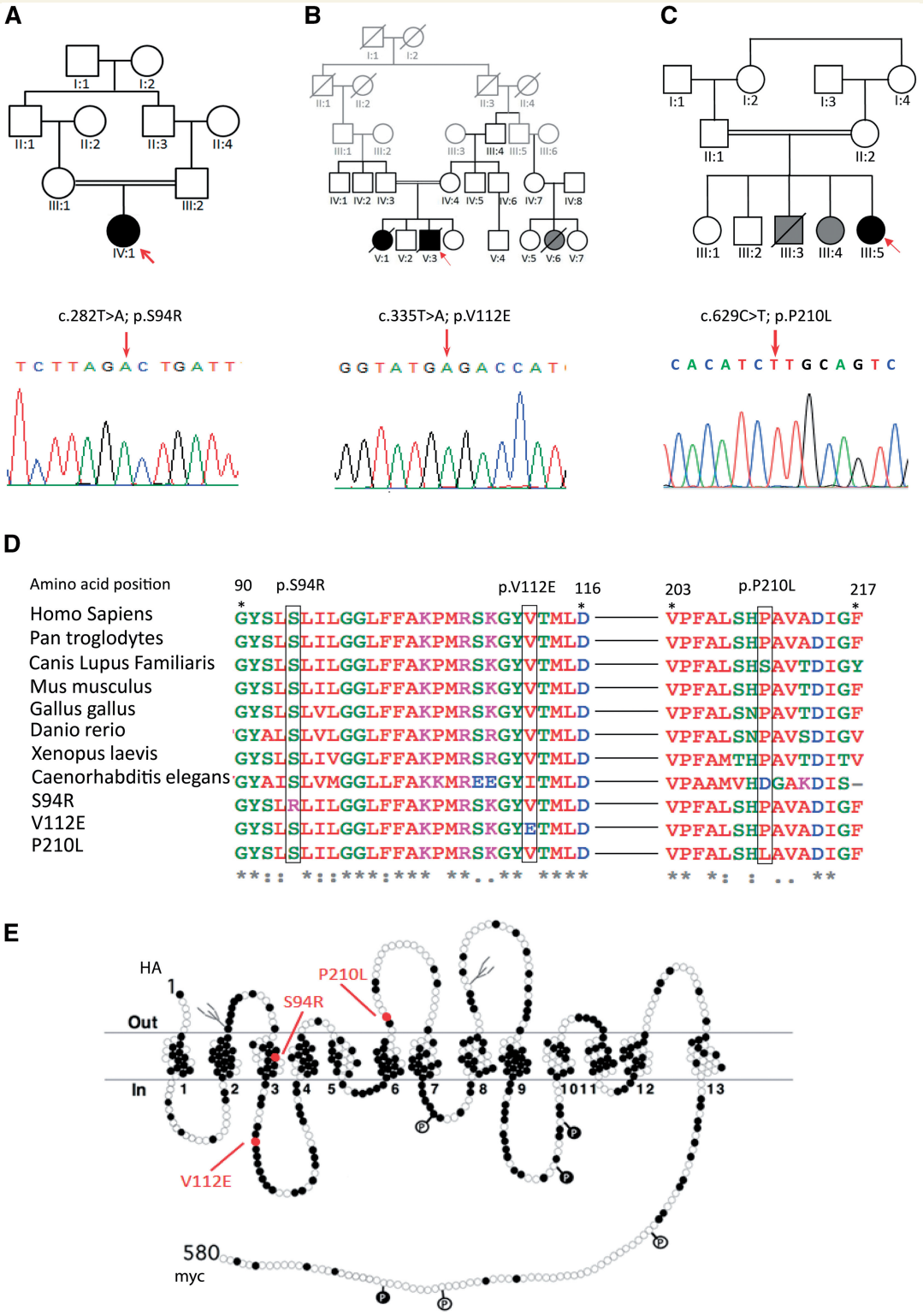

Figure 1 Family pedigrees, and mutations detected in *SLC5A7*. (**A–C**) Family pedigrees and whole-exome sequencing results. Whole-exome sequencing was done for affected members of each family (Family 1 Patient IV:1, Family 2 Patient V:3 and Family 3 Patient III:5) revealed a single novel deleterious homozygous variant in each subject in the same gene *SLC5A7*. For Family 3, two siblings (Patients III:3 and III:4) affected with a separate genetic disorder (Fowler syndrome) are marked out in grey. (**D**) Sequence alignment displays both affected residues (p.Ser94Arg and p.Val112Glu) high evolutionarily sequence conservation while p.Pro210Leu less conserved. (**E**) CHT topology. The 580 amino acid CHT protein has 13 transmembrane spanning domains and the N-terminus is extracellular while C-terminus is intracellular. The three amino acid substitutions from the missense mutations are indicated in brackets. Two sets of constructs are used in this study, the tags of each set are marked out at the termini.

Table 1 Clinical details of affected patients

	Family 1	Family 2		Family 3
Pedigree ID	**Patient IV:1**	**Patient V:1**	**Patient V:3**	**Patient III:5**
Mutation	NM_021815.2 c.282 T>A; p.Ser94Arg	NM_021815.2 c.335T>A; p.Val112Glu	NM_021815.2 c.335T>A; p.Val112Glu	NM_021815.2 c.629 C>T; Pro210Leu
Gender	Female	Female	Male	Female
Ethnicity	Turkish	Hispanic	Hispanic	Somalian
Age of latest exam, years	2.5	Deceased at 11 months	Deceased age 6 months	3.5
Birth gestation, birth weight, OFC	32 w, 1676 g (50th centile), 30 cm (60th centile)	40 w, 2760 g (10th centile)	38 w, 2985 g (75th centile)	37 w, 2515 g (10-25th centile), 33 cm (50th centile)
Presentation at birth	Floppy infant, lack of respiratory effort, ventilator dependent, swallowing difficulties	Floppy infant, lack of respiratory effort, ventilator dependent, swallowing difficulties	Floppy infant, lack of respiratory effort, ventilator dependent, swallowing difficulties	Floppy infant, respiratory insufficiency, ventilated, swallowing difficulties
Neurological features	Severe global developmental delay Motor reaction to sensory stimuli without orientation Severe muscular hypotonia Generalized muscle atrophy Minimal spontaneous and non-purposeful antigravity movements Bulbar insufficiency	Severe global developmental delay Severe muscular hypotonia Bulbar insufficiency Seizures	Severe global developmental delay Severe muscular hypotonia	Severe muscular hypotonia Fatigability, independent sitting Global developmental delay Myoclonic jerks with EEG features
Respiratory features	Continuous ventilation via tracheostomy	Continuous ventilation via endotracheal intubation	Continuous ventilation via tracheostomy	Continuous ventilation via tracheostomy
Gastrointestinal features	Gastrostomy	Bowel perforations (recurrent)	Bowel perforations (recurrent)	Gastrointestinal reflux, Recurrent diarrhoea, Gastrostomy for swallowing difficulties
Ocular features	Ophthalmoplegia, ptosis	Not available/not reported	Not available/not reported	Ophthalmoplegia, ptosis
Neuroimaging	Generalized atrophy of the brain (brain MRI, 2.5 years)	Normal (cranial U/S at birth)	Normal (brain MRI)	Subcortical cysts (brain MRI, 2 months)
Nerve conduction studies/ EMG	Repetitive stimulation revealed no responses from both median and tibialis nerves	Not available	Widespread fibrillation in limb and trunk muscles with no voluntary motor unit activity. The motor CMAP were severely reduced with relatively preserved conduction velocities	Repetitive stimulation at 2 months of age of N. ulnaris, M. abductor digiti minimi dx. At rest, nerve stimulation (3 Hz) × 10 times resulted in 84% decrement. A marked reduction in decrement was noted after administration of high dose edrophonium, resulting in 17% decrement.

(continued)

Table 1 Continued

	Family 1	Family 2		Family 3
Pedigree ID	**Patient IV:1**	**Patient V:1**	**Patient V:3**	**Patient III:5**
Muscle histology	Myopathic changes, loss of fibre typing, atrophic fibres, targetoid areas on electron microscopy (muscle biopsy at 5 month of age)	Generalized muscle atrophy	Myofibres seem to vary little in shape; scattered myofibres showing segmental granularity with loss of cross sections; electron microscopy of the skeletal muscle fibres showed changes compatible with targetoid fibres: focal loss of Z-bands, unsynchronized contractile elements, and jumbled contractile elements	Not performed
EEG	Reduced activity and few spikes	Left occipital and temporal epileptiform discharges with occasional right temporal lobe discharges	In neonatal period, frequent spikes and sharp waves from the right temporal region at times clustering in a semi-rhythmic fashion up to 10 s. Some sharp wave activity was independently observed in the right central (C4) and over the central vertex (CZ) areas	Epileptiform activity, (normalized at age 2 years on levetiracetam treatment)
Treatment and response	In neonatal period no response to 3 days of pyridostigmine trial	Not available/not reported	Not available/not reported	Positive test result: edrophonium (Tensilon®), pyridostigmine: improved tone and muscle function, with increased spontaneous movements of limbs and decrease in ophthalmologic symptoms Addition of 3,4-diaminopyridine: no effect and was terminated Ephedrine: positive effect on spontaneous motor activity in limbs and on respiratory function, additional to that of pyridostigmine

CMAP = compound muscle action potential; dx = dextra; EEG = electroencephalogram; OFC = occipitofrontal circumference; U/S = ultrasound; w = weeks.

antigravity movements observed and this individual was unable to follow objects with her eyes or give oriented response to stimuli. Progressive brain atrophy was revealed by serial neuroimaging (Supplementary Fig. 3). A positive Tensilon test was seen in one child (Family 3, Patient III:5), who was treated with pyridostigmine from 2 months of age, which significantly improved the hypotonia and ophthalmoplegia. The fatigable nature of the muscle weakness became more obvious in Patient III:5 of Family 3 with increasing age and gross motor development. 3,4-diaminopyridine was added to the treatment without any benefit; however, ephedrine treatment showed additional benefit to pyridostigmine on fatigability and muscle force. Continued respiratory insufficiency and gastrointestinal symptoms remain and she has a tracheostomy and gastrostomy *in situ*. At age 3.4 years, although she is unable to vocalize and it was difficult to systematically assess her cognitive ability, she communicates by signing to indicate her needs, and she is able to interact like a 2.5-year-old child.

In addition to the swallowing difficulties seen in all four affected children, gastrointestinal motility issues were a peculiar clinical feature of the siblings in Family 2 (Patients V:1 and V:3) who suffered recurrent bowel perforations. Electroencephalogram abnormalities were observed in all affected individuals, ranging from slowing of activity reflecting brain atrophy without pathological discharges to episodes of spikes and sharp waves resembling seizure-like activity. A muscle biopsy was performed in two individuals (Family 1 Patient IV:1 and Family 2 Patient V:3) in infancy and revealed targetoid-fibre like muscle lesions. See Table 1 and Supplementary material for detailed clinical summaries of each patient.

Genetic studies

To define the disease-causing mutations, we undertook whole-exome sequencing of affected members of each family (Family 1 Patient IV:1; Family 2 Patients V:1 and V:3; and Family 3 Patient III:5) to generate candidate variant profiles. This identified a single, novel homozygous *SLC5A7* missense variant in each subject as the most likely cause of their condition, specifically c.282T>A/p.Ser94Arg in Family 1, c.335T>A/p.Val112Glu in Family 2, and c.629C>T/p.Pro210Leu in Family 3 (NM_021815) (Fig. 1A–C). The p.Ser94 and p.Val112 residues are stringently conserved in evolution, while the p.Pro210 residue is located in the less well conserved sixth transmembrane-spanning region. Each sequence variant results in an amino acid substitution (Fig. 1D and E), which shows high damage prediction using *in silico* prediction programs. Each alteration was validated by dideoxy sequencing and found to co-segregate appropriately in each family according to recessive mode of inheritance, and none are present in online genomic databases (1000 Genomes, Exome Variant Server, Exome Aggregation Consortium databases and the Greater Middle Eastern Variome Database).

CHT expression studies

To assess the outcome of CHT mutation on transporter function, we first undertook heterologous expression studies of mutant and wild-type CHT constructs using transiently-transfected HEK 293T cells. In our previous study to detect expression of wild-type as well as mutant (p.Lys499Asnfs*13) CHT, which we found to be associated with dHMN-VII (Barwick *et al.*, 2012), a haemagglutinin (HA) tag was added to the N-termini of both transporters (HA-CHT^{WT}). To maintain experimental continuity, constructs were produced in the same plasmid vector (pRK5) with the HA-tag included, in parallel with an additional set of constructs generated in a pCMV6 plasmid vector with C-terminal double myc- and FLAG-tags. For additional continuity across our dataset, mutant constructs were produced to undertake experiments for the substitutions affecting human residues Ser94 and Val112, as only these residues are located in regions highly conserved in *C. elegans*, for functional studies in this species (see below).

Western blot analysis of HEK 293T cell lysates transiently transfected with myc-tagged wild-type or mutant CHT constructs showed that for equivalent amounts of cDNA transfected, approximately equal levels of polypeptide were produced, suggesting that these variants do not notably alter translation or protein stability (Supplementary Fig. 5A). To determine whether cell surface localization may be affected by the missense mutations, we isolated cell surface proteins after biotinylation followed by NeutrAvidin agarose pulldown. Western blotting showed reduced surface expression of all three missense mutations in contrast to wild-type transporters (Supplementary Fig. 5B). This finding was further confirmed by assessing CHT expression under permeabilized or non-permeabilized conditions in HEK 293T cells transfected with HA-CHT^{WT}, HA-CHT^{S94R}, and HA-CHT^{V112E}, HA-CHT^{P210L} analysed for total and surface protein signal by ELISA (Fig. 2A and B).

Immunofluorescence staining of transiently transfected HEK 293T cells revealed a predominantly intracellular vesicular localization of CHT^{WT}-MYC, CHT^{S94R}-MYC, and CHT^{V112E}-MYC, CHT^{P210L}-MYC with a small fraction of proteins on the plasma membrane (Supplementary Fig. 4) consistent with previous findings in cultured cells (Okuda *et al.*, 2002; Ferguson *et al.*, 2003; Ribeiro *et al.*, 2003; Nakata *et al.*, 2004). We also observed a higher abnormal expression ratio of the mutants CHT-MYC^{S94R} and CHT-MYC^{V112E} as revealed by increased number of HEK 293T cells containing larger aggregates or vesicles >1 µm in the cell body localization compared with wild-type (~20% increase, Supplementary Fig. 4G). This indicates a destabilizing effect of the missense mutation on CHT. Moreover, we found that these CHT aggregates co-localized with lysosomes (Supplementary Fig. 4C and E). To gain better understanding of CHT and mutant localization in cells similar to neurons, PC12 neuroblastoma cells were transfected with CHT^{WT}-MYC, CHT^{S94R}-MYC, and CHT^{V112E}-MYC, CHT^{P210L}-MYC constructs, with results

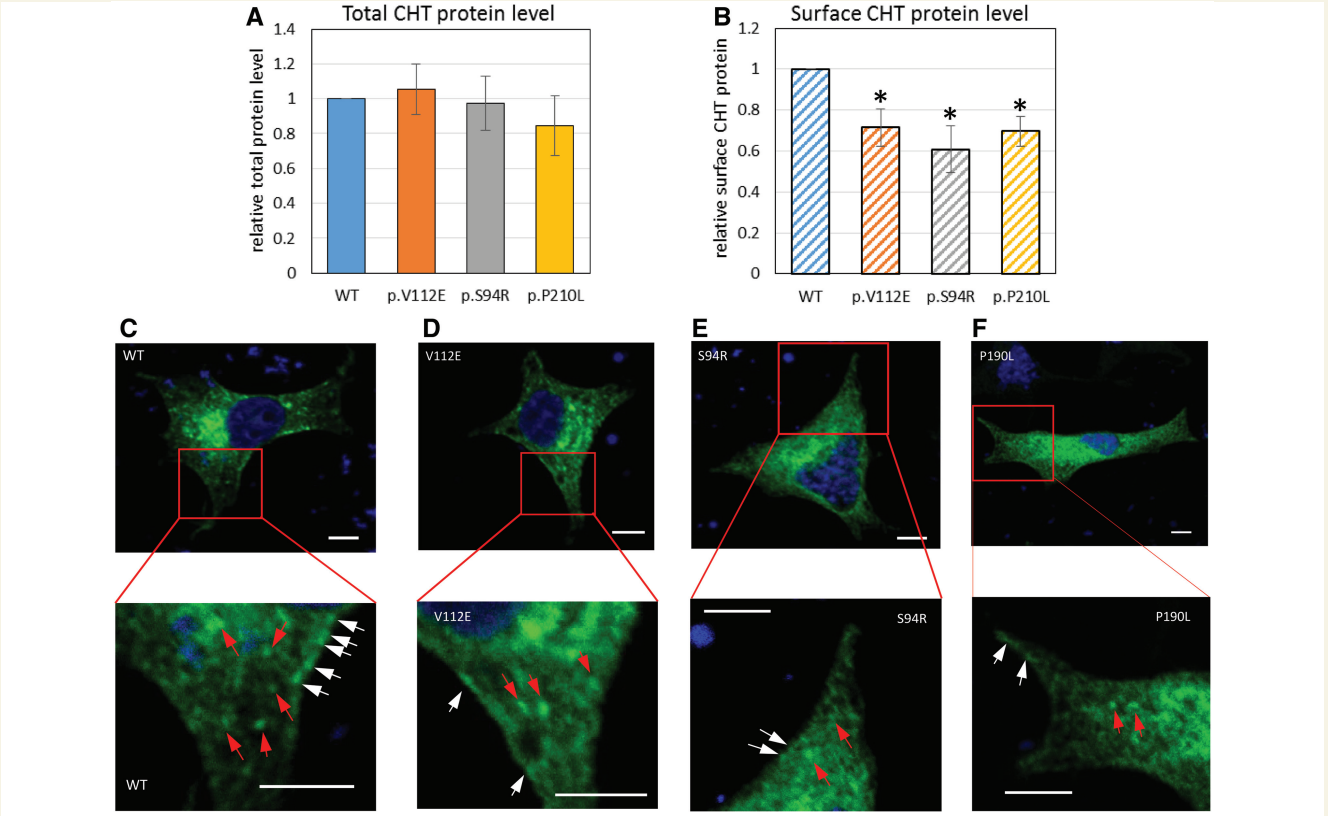

Figure 2 Recessive CHT missense mutations lead to reduced membrane localization. (**A** and **B**) The total and surface N-terminal HA-CHT protein level was assessed by ELISA as described in (Bogatcheva *et al.*, 2007). Protein level is shown in arbitrary units (AU) as a ratio of specific horseradish peroxidase (HRP) activity of mutant to wild-type CHT after anti-HA-HRP antibody binding, (**A**) total CHT protein level and (**B**) surface CHT protein level, which is also further normalized to total protein expression. Results are presented as means ± standard error (SE) ($n = 3$, $^*P < 0.05$, one-way ANOVA). (**C–F**) CHT cellular localization in PC12 cells transfected with CHT^{WT}-MYC (**C**), CHT^{S94R}-MYC (**D**), and CHT^{V112E}-MYC (**E**), CHT^{P210L}-MYC (**F**) expression constructs. Transient expressed myc-tagged CHT in transfected PC12 cells was detected via immunostaining using myc antibody (green). Nucleus is stained in DAPI (blue). Scale bar = 5 μm. *Bottom* panels show magnified view of the red square area of the corresponding *top* panel. CHT^{WT}-MYC (**C**) has intracellular vesicular localization (red arrows) and very clear membrane localization (white arrows). CHT^{V112E}-MYC (**D**) has similar intracellular localization but decreased membrane localization compared to CHT^{WT}-MYC. CHT^{S94R}-MYC (**E**) and CHT^{P210L}-MYC (**F**) do not show significant vesicular and membrane localization.

again revealing a predominantly vesicular localization with a minor proportion of CHT expression on the cell membrane (Fig. 2C–F) as previously described (Ribeiro *et al.*, 2003). However, compared to CHT^{WT}-MYC, which has a visible clear membrane and vesicular localization (Fig. 2C), reduced membrane localization together with diffuse vesicular localization was observed in other CHT mutants (Fig. 2D–F and Supplementary Fig. 7), particularly CHT^{S94R}-MYC, which exhibited almost no visible membrane localization (Fig. 2E and Supplementary Fig. 7). Additionally, we also noticed that CHT^{V112E}-MYC exhibits similar intracellular vesicular features to CHT-MYC^{WT} with admixtures of small vesicles of different sizes, while CHT^{S94R}-MYC and CHT^{P210L}-MYC exhibited fewer vesicular features. We performed a series of co-localization studies using markers for the endoplasmatic reticulum, Golgi apparatus, endosomes, synaptic vesicles and lysosomes (Supplementary Fig. 6A–E). A more detailed inspection of the intracellular vesicles in CHT-myc expressing PC12 cells revealed that CHT-MYC^{WT} co-localizes well with synapsin 1 and also with Rab7 (Supplementary Fig. 6A and B), consistent with previous studies (Ribeiro *et al.*, 2007). The other three mutants displayed less overlap with synapsin 1 and Rab7 markers, but increased overlap with Lamp1 (Supplementary Fig. 6C) suggestive of dysfunctional CHT mutant vesicles, possibly fusing with lysosomes for degradation.

Together these findings indicate that mutations in the CHT transmembrane region are likely to impair localization of mutant CHT to the cell surface in both PC12 and HEK 293T cells and lead to destabilization of the protein, resulting in reduced CHT levels at the plasma membrane.

In vivo Caenorhabditis elegans CHT trafficking assays

To gain additional insight into the impact of the CHT sequence variants *in vivo*, we took advantage of the high

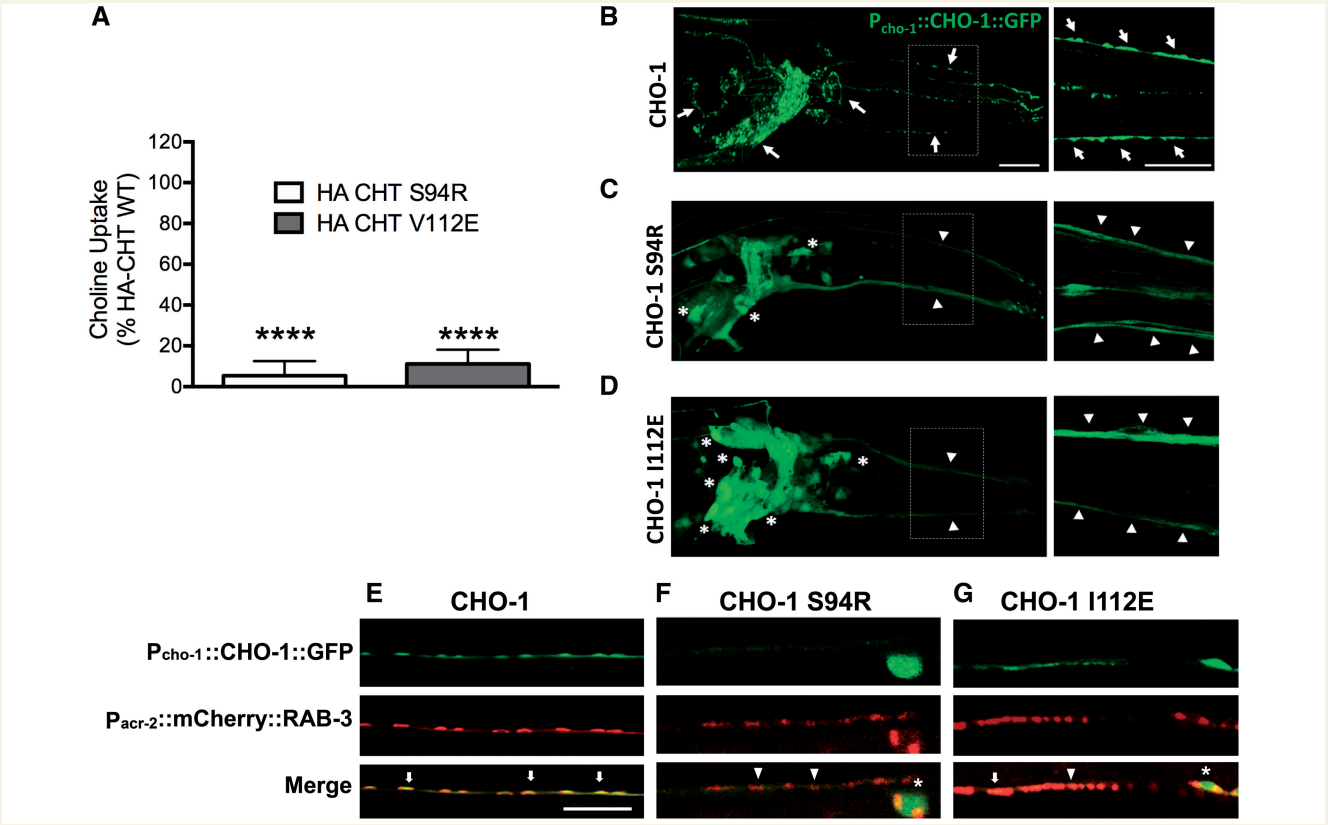

Figure 3 Recessive CHT missense mutation results in altered synaptic localization and have several reduced uptake activity. (**A**) Choline transport activity is significantly reduced in cells transfected with mutant (p.Val112Glu and p.Ser94Arg) versus wild-type constructs. CHT activity was diminished for both mutants p.Ser94Arg and p.Val112Glu compared to wild-type CHT (HA-CHT^{S94R}: $n = 4$, $^*P < 0.0001$; HA-CHT^{V112E}: $n = 4$, $^*P < 0.0001$, one-way ANOVA, Dunnett's *post hoc* test). Specific choline uptake was determined by subtracting the uptake obtained in transfected cells with that of mock (vector) transfected cells obtained in assays conducted in parallel. (**B**) Wild-type Pcho-1::CHO-1::GFP localization and expression *in vivo* in cholinergic neuron cell bodies and synapses in *C. elegans*. *Right panel*: Increased magnification (dotted line box) with arrows indicating normal CHO-1 trafficking as revealed by a punctate labelling patterning in neuronal processes. Scale bar = 20 μm. (**C**) Expression of CHO-1 Ser94Arg GFP-tagged protein under the expression of the *cho-1* native promoter. The mutated protein appears diffuse in neuronal processes and significantly trapped in cell bodies of cholinergic neurons (indicated by asterisks). *Right panel*: Increased magnification (dotted line box) indicates that mutated CHO-1 does not localize to synaptic regions in neuronal processes. The florescent intensity is ~3-fold lower than wild-type when injected at similar concentration (adjusted acquisition is shown). (**D**) Expression of CHO-1 Ile112Glu GFP-tagged protein, under expression of *cho-1* native promoter. The mutated protein appears diffuse in neuronal processes and partially trapped in cell bodies of some cholinergic neurons (indicated by asterisks). *Right panel*: Increased magnification (dotted line box) where mutated CHO-1 does not exhibit GFP puncta in neuronal processes, indicating the absence of proper CHO-1 localization in synaptic vesicles. (**E–G**) Mutated P_{cho-1}::CHO-1::GFP localization and expression *in vivo* in the *C. elegans* cholinergic motor neurons. (**E**) Wild-type CHO-1 protein, expressed under the *cho-1* native promoter, exhibits normal co-localization with cholinergic neuron synaptic marker, P_{acr-2}::mCherry::RAB-3 (arrows). Whereas (**F**) CHO-1 Ser94Arg and (**G**) CHO-1 Ile112Glu GFP-tagged proteins expressed under the *cho-1* native promoter lack the complete synaptic co-localization observed in wild-type protein expression (arrowheads), with CHO-1 Ile112Glu showing occasional correct localization (arrow). CHO-1 Ser94Arg and CHO-1 Ile112Glu mutant proteins appear to be partially trapped in the cell bodies (asterisks).

degree of conservation of essential features of CHT neurotransmission between the nematode *C. elegans* and humans (Nonet, 1999). Because of the simplicity of this genetically tractable system, the *C. elegans* model offers an important opportunity to investigate the functional impact of genetic variants on CHT trafficking. Importantly, the polypeptide region encompassing two of the residues mutated in our studies is highly conserved in the worm, enabling us to investigate these substitutions (p.Ser94Arg and p.Val112Glu; *C. elegans* p.Ile112Glu) via expression of wild-type and mutant transporter proteins as GFP fusions (Fig. 3B–D). In previous studies, Matthies *et al.* (2006) demonstrated that CHO-1 localizes to cholinergic synapses when expressed via the endogenous *cho-1* promoter. Animals were co-injected with a RAB-3:mCherry fusion construct to identify transporter localization in relation to cholinergic synapses (Fig. 3E–G). These studies, undertaken at different injection concentrations (70 ng/μl, 20 ng/μl, 5 ng/μl), consistently revealed an almost complete loss of export of the CHT variants into the axonal processes of head cholinergic neurons

and in the cholinergic ventral cord motor neurons (Fig. 3C and F for p.Ser94Arg and Fig. 3D and G for p.Ile112Glu), resulting in an absence of detectable mutant CHT from synapses with mutant molecule remaining restricted to the cell body.

CHT transporter activity assays

Finally, we investigated the outcome of the missense sequence variants on CHT transporter activity using ^{3}H-choline transport assays in transiently transfected HEK 293T cells as previously (Barwick *et al.*, 2012) for the residues for which parallel *C. elegans* transporter studies were also possible, to provide consistent interpretation of trafficking outcomes. As shown in Fig. 3A, CHT activity was diminished for both mutants p.Ser94Arg and p.Val112Glu compared to wild-type CHT (HA-CHT^{S94R}: $n = 4$, $P < 0.0001$; HA-CHT^{V112E}: $n = 4$, $^{*}P < 0.0001$, one-way ANOVA, Dunnett's *post hoc* test).

Discussion

The high affinity CHT transporter consists of 580 amino acids predicted to organize into 13 transmembrane domains, with an extracellular NH_2 terminus and intracellular COOH terminus (Fig. 1E). CHT is primarily responsible for choline uptake at the NMJ (Ferguson *et al.*, 2004) and is the rate-limiting step in acetylcholine synthesis and release (Apparsundaram *et al.*, 2000; Okuda and Haga, 2000). Consistent with this role, CHT is enriched *in vivo* at nerve terminals and is localized at the cell membrane and in synaptic vesicles (Ferguson and Blakely, 2004). Our *in vitro* and *in vivo* CHT trafficking and activity studies described here indicate that recessive CHT mutations are likely to confer at least two deleterious outcomes and significantly impair both CHT trafficking and export to synapses, leading to significantly compromised transporter function. Together, these outcomes are likely to result in profound reductions in transporter activity in affected infants, leading to the severe presynaptic CMS observed in our patients. Extremely low levels of mutant CHT at the NMJ would likely explain the extreme hypotonia, fatigability, lack of antigravity movements and respiratory insufficiency observed at birth. The cholinergic synapses continue to mature and develop after birth and any impact on respiration, gastrointestinal or bulbar function is subsequently magnified during the newborn period. Respiratory function is also compromised by apnoeic spells, possibly caused by alterations of cholinergic signalling of central neurons in the brainstem regulating breathing (Schara *et al.*, 2010; Bauché *et al.*, 2016). With increasing age, increased activity levels and gross motor development, the myasthenic component becomes more prominent with muscle fatigability in Patient III:5 of Family 3 affecting movement due to the increase in CHT activity requirement at the NMJ. Additionally, our findings may provide insight regarding possible mutant protein functionality–phenotype correlations as the most severe phenotype of infantile death and/or severe global neurodevelopmental delay [infant Patients Family 2 V:3 and Family 1 IV:1] associated with p.Val112Glu and p.Ser94Arg sequence variants located in the stringently conserved regions of CHT, lead to particularly severe CHT transport defects to the cell synapse and surface localization (Figs 2 and 3). Conversely, the individual harbouring the p.Pro210Leu substitution (Family 3, Patient III:5), located in the less evolutionarily conserved sixth transmembrane polypeptide region of CHT prohibiting a consistent evaluation of trafficking and transporter outcomes in *C. elegans*, was able to achieve sitting and is reported to be developing cognitively. The milder phenotype of the homozygous p.Pro210Leu harbouring patient is also consistent with the alterations in our transporter expression and membrane localization studies in different cells (Fig. 2 and Supplementary Figs 5, 6A–E and 7). Notably, treatment in this individual with pyridostigmine and ephedrine seemed to be beneficial whereas 3,4-aminopyridine appeared not to have any beneficial effects, a finding that was also documented by Bauché *et al.* (2016), who recently reported six children with CMS disorders and CHT mutations. Any defect of cholinergic neurotransmission would also be expected to impact on autonomic nervous system function, which may provide a plausible explanation for the gastrointestinal motility and bowel perforation observed in affected individuals. Apart from the clinical features likely due to dysfunctional transmission at the peripheral NMJ, notably affected individuals in Families 1 and 2 also show severe global neurodevelopmental delay with cognitive impairment and in Family 1 Patient IV:1, brain atrophy. Although brain atrophy and CNS impairment could result from prolonged hypoxia secondary to respiratory insufficiency, the child received immediate respiratory support and there was no indication or history of prolonged asphyxia or hypoxia reported. An effect on brain and cognitive development is consistent with a requirement for CHT function in the cholinergic neurons of the CNS being essential for normal cognitive and neurobehavioural development (Berse *et al.*, 2005; Liu *et al.*, 2016). Consistent with this, a similarly variable impact on cognitive involvement including progressive brain atrophy has been described in patients with *CHAT* mutation, also responsible for a presynaptic CMS (Schara *et al.*, 2010).

The clinical outcome and nature of the autosomal recessively-acting CHT missense mutations described here overlap with and extend the clinical outcomes recently described due to autosomal recessively-acting *SLC5A7* mutations in a CMS-spectrum condition (Bauché *et al.*, 2016), to a more severe impact on brain development associated with early infantile lethality and brain atrophy, as well as abnormal gastrointestinal function. Together these clinical findings and molecular outcomes contrast with those of our previous investigations of dominantly-transmitted dHMN-

VII, which we found to be associated with a single base deletion (c.1497delG: p.Lys499Asnfs*13) in *SLC5A7* (Pridmore *et al.*, 1992; McEntagart *et al.*, 2001; Dick *et al.*, 2008; Barwick *et al.*, 2012), entailing a near-complete deletion of the transporter's cytoplasmic C-terminus. While this form of hereditary motor neuropathy is also associated with vocal cord paresis, affected individuals display no neurological symptoms early in life and typically present clinically with motor neuron signs only during the second or third decade of life; hypotonia and muscle fatigability is not, to our knowledge, a feature of dHMN-VII. The data presented in the current manuscript extend these existing datasets and provide a potential explanation for the distinct modes of inheritance, and clinical outcomes associated with both classes of CHT mutation. Our cell surface expression and *C. elegans* axonal transport data indicate that the mutant CHTs studied are likely to be inefficiently transported to NMJ synapses. This may indicate that CHTs bearing transmembrane missense substitutions are effectively 'filtered' and prevented from reaching the NMJ, averting opportunities for dominant-negative interference arising from oligomerization with wild-type molecules. This may likely explain the lack of clinical outcome in heterozygous carrier parents in whom CHT activity arising from the single wild-type allele appears to be sufficient for physiological function. Conversely, the severe clinical outcome exhibited by bi-allelic missense mutant individuals likely reflects the collective outcomes on overall CHT activity at the NMJ stemming from reduced CHT transporter membrane availability of the mutant proteins, in combination with severely impaired transporter activity. Indeed, the phenotype in individuals with bi-allelic recessive CHT mutation is comparable with the phenotype of the *Slc5a7* knock-out in the mouse, which results in mice born in Mendelian ratios that become immobile, have irregular breathing, appear cyanotic, and die shortly after birth due to respiratory failure, immobility and failure to feed (Ferguson *et al.*, 2004; Ferguson and Blakely, 2004).

We have identified recessively acting *SLC5A7* mutations associated with a severe form of presynaptic CMS impacting brain development and cognitive function, likely due to the combined deleterious outcomes on both CHT trafficking and transporter activity. Taken together with our earlier published studies (Barwick *et al.*, 2012), we define distinct classes of CHT mutations associated with wide-ranging neurological outcomes, and provide a putative mechanistic explanation for the differing modes of inheritance, disease mechanisms and clinical presentation of each disorder. These findings provide an important basis from which to consider therapeutic approaches involving pharmacological chaperones to enhance CHT activity at the NMJ, and potentially make best use of existing treatment therapies.

Web resources

The URLs for data presented herein are as follows:
Online Mendelian Inheritance in Man (OMIM), http://www.omim.org
Clustal Omega, http://www.ebi.ac.uk/Tools/msa/clustalo/
PolyPhen-2, http://genetics.bwh.harvard.edu/pph2/
Mutation Taster, http://www.mutationtaster.org/
ExAC, http://exac.broadinstitute.org/

Acknowledgements

The authors would like to thank the families described herein for participating in our study. We thank Cassandra Retzlaff and Qiao Han for assistance with the CHT uptake assay and Peter Rodriguez for *C. elegans* laboratory support. We thank Dr Natalia Kononenko (CECAD, Cologne) for the organelle constructs and antibodies. Special thanks also to the family of J.M. for supporting this work.

Funding

The study to A.C. was supported by the Medical Research Council (G1002279), NEWLIFE Foundation, and the Neurosciences Research Foundation. S.C. was supported by the Muscular Dystrophy Association/USA and by Deutsche Forschungsgemeinschaft/Germany (CI 218/1-1). R.B. was supported by National Institutes of Health award MH095044.

Supplementary material

Supplementary material is available at *Brain* online.

References

Ahmed MY, Al-Khayat A, Al-Murshedi F, Al-Futaisi A, Chioza BA, Pedro Fernandez-Murray J, et al. A mutation of EPT1 (SELENOI) underlies a new disorder of Kennedy pathway phospholipid biosynthesis. Brain 2017; 140: 547–54.

Apparsundaram S, Ferguson SM, George AL, Jr, Blakely RD. Molecular cloning of a human, hemicholinium-3-sensitive choline transporter. Biochem Biophys Res Commun 2000; 276: 862–7.

Arredondo J, Lara M, Gospe SM, Jr, Mazia CG, Vaccarezza M, Garcia-Erro M, et al. Choline acetyltransferase mutations causing congenital myasthenic syndrome: molecular findings and genotype-phenotype correlations. Hum Mutat 2015; 36: 881–93.

Barwick KE, Wright J, Al-Turki S, McEntagart MM, Nair A, Chioza B, et al. Defective presynaptic choline transport underlies hereditary motor neuropathy. Am J Hum Genet 2012; 91: 1103–7.

Bauché S, O'Regan S, Azuma Y, Laffargue F, McMacken G, Sternberg D et al. Impaired presynaptic high-affinity choline transporter causes a congenital myasthenic syndrome with episodic apnea. Am J Hum Genet 2016; 99: 753–61.

Berse B, Szczecinska W, Lopez-Coviella I, Madziar B, Zemelko V, Kaminski R, et al. Expression of high affinity choline transporter during mouse development *in vivo* and its upregulation by NGF and BMP-4 in vitro. Brain Res Dev Brain Res 2005; 157: 132–40.

Bogatcheva NV, Ferlin A, Feng S, Truong A, Gianesello L, Foresta C, et al. T222P mutation of the insulin-like 3 hormone receptor LGR8 is associated with testicular maldescent and hinders receptor expression on the cell surface membrane. Am J Physiol Endocrinol Metab 2007; 292: E138–44.

Dick KJ, McEntagart M, Alwan W, Reilly M, Crosby AH. Refinement of the locus for distal hereditary motor neuronopathy VII (dHMN-VII) and exclusion of candidate genes. Genome 2008; 51: 959–62.

Engel AG, Shen XM, Selcen D, Sine SM. Congenital myasthenic syndromes: pathogenesis, diagnosis, and treatment. Lancet Neurol 2015; 14: 461.

Feng Z, Ko CP. The role of glial cells in the formation and maintenance of the neuromuscular junction. Ann N Y Acad Sci 2008; 1132: 19–28.

Ferguson SM, Bazalakova M, Savchenko V, Tapia JC, Wright J, Blakely RD. Lethal impairment of cholinergic neurotransmission in hemicholinium-3-sensitive choline transporter knockout mice. Proc Natl Acad Sci USA 2004; 101: 8762–7.

Ferguson SM, Blakely RD. The choline transporter resurfaces: new roles for synaptic vesicles? Mol Interv 2004; 4: 22–37.

Ferguson SM, Savchenko V, Apparsundaram S, Zwick M, Wright J, Heilman CJ, et al. Vesicular localization and activity-dependent trafficking of presynaptic choline transporters. J Neurosci 2003; 23: 9697–709.

Herrmann DN, Horvath R, Sowden JE, Gonzalez M, Sanchez-Mejias A, Guan Z, et al. Synaptotagmin 2 mutations cause an autosomal-dominant form of lambert-eaton myasthenic syndrome and nonprogressive motor neuropathy. Am J Hum Genet 2014; 95: 332–9.

Holmstrand EC, Lund D, Cherian AK, Wright J, Martin RF, Ennis EA et al. Transgenic overexpression of the presynaptic choline transporter elevates acetylcholine levels and augments motor endurance. Neurochem Int 2014; 73: 217–28.

Liu X, Shi Y, Niu B, Shi Z, Li J, et al. Polymorphic variation in CHAT gene modulates general cognitive ability: an association study with random student cohort. Neurosci Lett 2016; 617: 122–6.

Matthies DS, Fleming PA, Wilkes DM, Blakely RD. The Caenorhabditis elegans choline transporter CHO-1 sustains acetylcholine synthesis and motor function in an activity-dependent manner. J Neurosci 2006; 26: 6200–12.

McEntagart M, Norton N, Williams H, Teare MD, Dunstan M, Baker P, et al. Localization of the gene for distal hereditary motor neuronopathy VII (dHMN-VII) to chromosome 2q14. Am J Hum Genet 2001; 68: 1270–6.

McKay BE, Placzek AN, Dani JA. Regulation of synaptic transmission and plasticity by neuronal nicotinic acetylcholine receptors. Biochem Pharmacol 2007; 74: 1120–33.

Nakata K, Okuda T, Misawa H. Ultrastructural localization of high-affinity choline transporter in the rat neuromuscular junction: enrichment on synaptic vesicles. Synapse 2004; 53: 53–6.

Nonet ML. Visualization of synaptic specializations in live C. elegans with synaptic vesicle protein-GFP fusions. J Neurosci Methods 1999; 89: 33–40.

Okuda T, Haga T. Functional characterization of the human high-affinity choline transporter. FEBS Lett 2000; 484: 92–7.

Okuda T, Okamura M, Kaitsuka C, Haga T, Gurwitz D. Single nucleotide polymorphism of the human high affinity choline transporter alters transport rate. J Biol Chem 2002; 277: 45315–22.

Okuda T, Osawa C, Yamada H, Hayashi K, Nishikawa S, Ushio T et al. Transmembrane topology and oligomeric structure of the high-affinity choline transporter. J Biol Chem 2012; 287: 42826–34.

Pridmore C, Baraitser M, Brett EM, Harding AE. Distal spinal muscular atrophy with vocal cord paralysis. J Med Genet 1992; 29: 197–9.

Ribeiro FM, Alves-Silva J, Volknandt W, Martins-Silva C, Mahmud H, Wilhelm A, et al. The hemicholinium-3 sensitive high affinity choline transporter is internalized by clathrin-mediated endocytosis and is present in endosomes and synaptic vesicles. J Neurochem 2003; 87: 136–46.

Ribeiro FM, Black SA, Cregan SP, Prado VF, Prado MA, Rylett RJ, et al. Constitutive high-affinity choline transporter endocytosis is determined by a carboxyl-terminal tail dileucine motif. J Neurochem 2005; 94: 86–96

Ribeiro FM, Pinthong M, Black SA, Gordon AC, Prado VF, Prado MA, et al. Regulated recycling and plasma membrane recruitment of the high-affinity choline transporter. Eur J Neurosci 2007; 26: 3437–48.

Sarter M, Parikh V. Choline transporters, cholinergic transmission and cognition. Nat Rev Neurosci 2005; 6: 48–56.

Schara U, Christen HJ, Durmus H, Hietala M, Krabetz K, Rodolico C, et al. Long-term follow-up in patients with congenital myasthenic syndrome due to CHAT mutations. Eur J Paediatr Neurol 2010; 14: 326–33.

Shen XM, Selcen D, Brengman J, Engel AG. Mutant SNAP25B causes myasthenia, cortical hyperexcitability, ataxia, and intellectual disability. Neurology 2014; 83: 2247–55.

Yis U, Baydan F, Karakaya M, Hız Kurul S, Cirak S. Importance of skin changes in the differential diagnosis of congenital muscular dystrophies. Biomed Res Int 2016; 2016: 3128735.